NPP-21/TPR is required for developmental control of spindle checkpoint strength in *C. elegans*

Natalie Gallagher[#], Shevelle Brown[#], Valentin Duprat[#], Simone Köhler*[§], Abby F. Dernburg*, and Needhi Bhalla[#]

[#]Department of Molecular, Cell and Developmental Biology, University of California, Santa Cruz, Santa Cruz, CA 95064

*Department of Molecular and Cell Biology, University of California, Berkeley, Berkeley, CA 94720

[§]Current address: Cell Biology and Biophysics Unit, European Molecular Biology Laboratory, 69117 Heidelberg, Germany

[1] corresponding author: nbhalla@ucsc.edu

Department of Molecular, Cell and Developmental Biology

225 Sinsheimer Labs

University of California, Santa Cruz

Santa Cruz, CA 95064

phone: (831) 459-1319

fax: (831) 459-3139

Running Title : NPP-21/TPR and checkpoint strength in the germline

18,550 characters

Abstract

The spindle checkpoint ensures accurate chromosome segregation by monitoring whether chromosomes, via kinetochores, are properly attached to the spindle. If chromosomes fail to establish bipolar attachment, the checkpoint delays the cell cycle to enable error correction. In *C. elegans* early embryos, activation of the spindle checkpoint produces a longer mitotic delay in primordial germ cells than somatic cells. We show that the conserved nucleoporin and spindle matrix component, NPP-21/TPR, is required for the stronger spindle checkpoint in germline cells. A checkpoint-proficient NPP-21::GFP transgene localizes to a spindle-like structure during mitosis and is enriched in germline cells, consistent with a cell-fate specific function for this protein. Finally, NPP-21 controls spindle checkpoint strength in germline cells via two, potentially linked, mechanisms: concentrating PCH-2 around mitotic chromosomes and promoting the localization of the checkpoint effector, Mad2, to unattached kinetochores. These experiments demonstrate a developmental role for NPP-21, and the spindle matrix, in controlling spindle checkpoint strength in immortal germline cells in *C. elegans*.

Introduction

The spindle checkpoint is a cell cycle surveillance mechanism that ensures that chromosomes are attached to the mitotic or meiotic spindle to guarantee accurate chromosome segregation and prevent aneuploidy. When chromosomes are unattached, a soluble, molecular signal halts or delays the cell cycle to allow for the defect to be corrected. Defects in spindle checkpoint components are associated with cancer progression (Kops et al., 2005; Matthews et al., 2022) and infertility (Baker et al., 2004; Huang et al., 2023; Zhang et al., 2020), highlighting their importance to human health.

The spindle checkpoint initiates from kinetochores, the specialized structures that assemble at centromeres to mediate microtubule attachment and proper chromosome segregation (Lara-Gonzalez et al., 2021). A complex of the conserved checkpoint factors, Mad1 and Mad2, binds unattached or incorrectly attached kinetochores. Mad2 adopts two functionally distinct conformations: an open, inactive form and a closed, active form. When Mad2 binds a specific motif, called the closure motif, in its binding partners, such as Mad1 and Cdc20, Mad2 undergoes a conformational conversion from inactive (open) to active (closed). At unattached kinetochores, the Mad1/Mad2 complex recruits additional inactive Mad2 so that it can bind Cdc20, adopting the active conformation and forming the Mitotic Checkpoint Complex, or MCC. The MCC sequesters Cdc20, a factor required to promote anaphase, to inhibit the cell cycle and allow time for error correction (Lara-Gonzalez et al., 2021). The evolutionarily ancient ATP-ase PCH-2/TRIP13 promotes spindle checkpoint function by ensuring the availability of open, inactive Mad2 (Ma and Poon, 2016; Ma and Poon, 2018; Nelson et al., 2015)

Despite the important role of the spindle checkpoint in preventing aneuploidy, the mitotic delay or arrest installed by the spindle checkpoint can be highly variable. The variability of the cell

68 cycle delay is called spindle checkpoint strength and depends on the number of unattached
69 kinetochores, cell volume, and cell fate (Collin et al., 2013; Galli and Morgan, 2016; Gerhold et
70 al., 2018; Kyogoku and Kitajima, 2017). For example, during early embryogenesis in *C. elegans*,
71 primordial germ cells have a stronger checkpoint than their somatic counterparts, independent
72 of their smaller size (Galli and Morgan, 2016; Gerhold et al., 2018), demonstrating
73 developmental differences in checkpoint strength. We showed that the stronger checkpoint in
74 germline cells depends on the asymmetric enrichment of the spindle checkpoint factor, PCH-
75 2/TRIP13 (Defachelles et al., 2020).
76
77 During mitosis in early *C. elegans* embryos, following nuclear envelope breakdown, PCH-
78 2::GFP and other checkpoint components, such as GFP::Mad1 and GFP::Mad2, remain
79 localized around mitotic chromosomes (Defachelles et al., 2020; Essex et al., 2009). This diffuse
80 localization resembles a structure known as the spindle matrix (Zheng, 2010). While the
81 composition and function of the spindle matrix remain controversial, some characterized spindle
82 matrix components interact with spindle checkpoint components (Lince-Faria et al., 2009;
83 Schweizer et al., 2013), making them attractive candidates to regulate spindle checkpoint
84 strength during development.
85
86 NPP-21/TPR is the *C. elegans* ortholog of the *Drosophila* spindle matrix protein, Megator, and
87 the human nucleoporin TPR. In *C. elegans*, NPP-21/TPR has been primarily characterized as a
88 nucleoporin, a member of a large family of proteins that form the nuclear pore and allow for
89 macromolecular transport between the cytoplasm and nucleus (Cohen-Fix and Askjaer, 2017).
90 NPP-21/TPR forms the nucleoplasmic face or basket of the pore (Cohen-Fix and Askjaer, 2017).
91 In *Drosophila*, Megator is a nucleoporin that also localizes to the area occupied by the miotic
92 spindle (Qi et al., 2004) and supports robust recruitment of Mad2 to unattached kinetochores
93 (Lince-Faria et al., 2009).

94

95 Here, we show that NPP-21/TPR, in its capacity as a spindle matrix component, is required for
96 developmental control of spindle checkpoint strength in *C. elegans*. A strain carrying both a
97 transgene of *npp-21*, *AID-3xFLAG::npp-21*, and the Arabidopsis TIR1 gene is functional for
98 checkpoint activation in somatic cells of the early embryo but cannot support the stronger
99 checkpoint in germline cells. When NPP-21 is acutely degraded, checkpoint strength is further
100 compromised in germline cells but has no effect on somatic cells. Consistent with this cell-fate
101 specific function, NPP-21::GFP consistently forms a structure that resembles the spindle matrix
102 during mitosis and is asymmetrically enriched in germline cells, compared to somatic cells.
103 Finally, NPP-21 ensures a stronger checkpoint in germline cells by concentrating PCH-2::GFP
104 around mitotic chromosomes and promoting the robust recruitment of GFP::Mad2 to unattached
105 kinetochores. We propose that during the rapid cell divisions of early embryogenesis, NPP-21,
106 and the spindle matrix, concentrate checkpoint factors around mitotic chromosomes to ensure
107 genomic integrity, a role that is particularly important in primordial germ cells that will give rise to
108 sperm and eggs.

109

110 **Results and Discussion**

111

112 **NPP-21 is required for the stronger spindle checkpoint in germline, P_1 cells**

113

114 NPP-21 is an essential gene (Piano et al., 2000). Therefore, to determine whether NPP-21
115 plays a role in the spindle checkpoint in early developing embryos, we exploited the auxin-
116 inducible degron system (AID) to acutely degrade NPP-21 in oocytes and early embryos. Using
117 CRISPR/Cas9, we generated a version of NPP-21 tagged at its N-terminus with the AID degron
118 and a 3xFLAG tag (*AID-3xFLAG::npp-21*, also referred to as *AID::npp-21*) in a strain that also
119 expresses the Arabidopsis TIR1 protein via a germline promoter (*Pgld-1::TIR1-mRuby)* (Zhang

120 et al., 2015). In the presence of auxin, TIR1 binds to degron-tagged proteins and targets them
121 for polyubiquitylation and degradation by the proteasome (Nishimura et al., 2009). In the
122 presence of ethanol and absence of auxin, this strain produces modest defects in in meiotic
123 chromosome segregation, illustrated by the elevated frequencies of inviable embryos and male
124 self-progeny (Table 1). When these worms were exposed to auxin, they produced few viable
125 progeny and 25% male self-progeny (Table 1). Thus, the *AID::npp-21* transgene is mostly
126 functional, with some slight defects in embryonic viability and meiotic chromosome segregation,
127 which may be the product of the tag and/or auxin-independent degradation. By contrast, auxin-
128 induced depletion of AID-3xFLAG::NPP-21 results in very high embryonic lethality and severe
129 defects in meiotic chromosome segregation, consistent with its essential role (Piano et al.,
130 2000).
131
132 We tested whether we could rapidly degrade AID-3xFLAG::NPP-21. We performed this
133 experiment in the most proximal oocytes undergoing cellularization (-1 oocyte). Upon
134 fertilization, these oocytes complete meiosis and enter mitosis to begin embryonic development
135 within an hour (Robertson and Lin, 2013). We exposed young adult hermaphrodites worms
136 undergoing oogenesis to auxin for one hour and performed indirect immunofluorescence
137 against the FLAG tag to visualize AID-3xFLAG::NPP-21. In worms exposed to ethanol, we
138 observed staining at the nuclear periphery in the most proximal oocytes, consistent with its
139 known role as a member of the nuclear pore complex (Figure 1A). After one hour of auxin
140 treatment, we could no longer detect AID-3xFLAG::NPP-21 at the nuclear periphery (Figure 1A),
141 indicating that we can reliably and rapidly degrade NPP-21 in oocytes that are about to be
142 fertilized and develop into embryos.
143
144 Having established this protocol, we used it to test whether degradation of NPP-21 affected
145 normal mitotic timing and spindle checkpoint function in early embryos, specifically two cell

146 embryos which have already differentiated into soma (AB cells) and germline (P_1 cells) (Figure
147 1B). We analyze mitotic timing by calculating the time between nuclear envelope breakdown
148 (NEBD) and the onset of cortical contractility (OCC), which coincides with anaphase in embryos
149 expressing an mCherry tagged histone, mCherry::H2B, and the plasma membrane marker,
150 GFP::PH (Essex et al., 2009). NEBD is visualized as the diffusion of soluble mCherry::H2B
151 signal from the nucleus and OCC is detected when the plasma membrane changes
152 conformation from circular to rectangular (Supplemental Figure 1A). In P_1 cells, it is difficult to
153 assess OCC and we used anaphase as an indicator of mitotic exit (Supplemental Figure 1A).
154 When transgenic *AID::npp-21* worms were exposed to ethanol or auxin, we did not detect any
155 difference in mitotic timing between ethanol-treated or auxin-treated worms, or with control
156 worms treated with ethanol, in either AB or P_1 cells, indicating that NPP-21 is not required for
157 unperturbed mitosis in either cell type (Figures 1C and D).
158
159 Next, we activated the spindle checkpoint in *AID::npp-21* AB cells by performing RNA
160 interference (RNAi) against *zyg-1*, a conserved cell cycle kinase required for centrosome
161 duplication (O'Connell et al., 2001). In the absence of *zyg-1*, two cell embryos only have one
162 centrosome and generate a monopolar spindle, producing chromosomes with unattached
163 kinetochores (Essex et al., 2009). In *zyg-1*^{RNAi} embryos, OCC is defined as the formation of
164 persistent membrane blebs between the AB and P_1 cells (arrows in Supplemental Figure 1A). In
165 AB cells of *zyg-1*^{RNAi} embryos, we observed a slight decrease in mitotic timing in transgenic
166 *AID::npp-21* worms on ethanol or auxin (Figure 1C), when compared to control embryos on
167 ethanol. This difference was not statistically significant, indicating that NPP-21 might play a role
168 in promoting a strong spindle checkpoint in AB cells but is not required for the checkpoint in
169 these cells. In contrast, when we activated the spindle checkpoint in P_1 cells in *AID::npp-21*
170 worms exposed to ethanol, these cells showed similar mitotic timing as AB cells treated with
171 *zyg-1* RNAi (Figures 1C and D) and a weaker checkpoint than control worms (Figure 1D).

172 These data indicate that either the transgenic *AID::npp-21* is not fully functional for spindle
173 checkpoint function in P_1 cells or that the presence of TIR1, even in the absence of auxin,
174 affects protein function. More importantly, these data suggest a role for NPP-21 in spindle
175 checkpoint strength in this specific cell type. When *AID::npp-21* worms are exposed to auxin for
176 more than one hour, we detected a further weakening of the spindle checkpoint (Figure 1D),
177 indicating that NPP-21 is required for a robust spindle checkpoint specifically in P_1 cells.
178
179 **NPP-21::GFP adopts a structure similar to the spindle matrix and is enriched in P_1 cells**
180
181 Given this cell fate-specific difference in the requirement for NPP-21 function in the spindle
182 checkpoint, we localized NPP-21::GFP in AB and P_1 cells in two cell embryos (Thomas et al.,
183 2023). First, we verified that *npp-21::gfp* worms were competent for checkpoint activation in AB
184 and P_1 cells. Because the presence of NPP-21::GFP prevented us from using GFP::PH to
185 monitor OCC, we measured mitotic timing using mCherry::H2B from NEBD to decondensation
186 of mitotic chromosomes (DECON) (Supplemental Figure 1B) (Essex et al., 2009). In embryos
187 expressing NPP-21::GFP, both AB and P_1 cells activated the spindle checkpoint and P_1 cells
188 displayed a stronger checkpoint than AB cells, similar to control worms (Figure 2A), verifying
189 that NPP-21::GFP is fully functional for checkpoint activation. Next, we localized NPP-21::GFP
190 and observed a striking difference in its localization in AB and P_1 cells. In 75% of two-cell
191 embryos (15/20), NPP-21::GFP remained in a cloud around mitotic chromosomes 120 seconds
192 after NEBD, a timepoint that corresponds to metaphase, in AB cells (see Materials and
193 Methods). In contrast to AB cells, after NEBD in P_1 cells, NPP-21::GFP reorganized around
194 mitotic chromosomes in a structure that resembled the mitotic spindle, similar to a spindle
195 matrix. In 25% of two cell embryos, both AB and P_1 cells exhibited this spindle-like localization
196 (Figure 2B). Thus, in P_1 cells 100% of the time, and in AB cells 25% of the time, NPP-21::GFP

197 adopts a localization pattern during mitosis that resembles the spindle matrix (see Supplemental
198 Movies).
199
200 We previously showed that PCH-2::GFP, which is required for spindle checkpoint function, is
201 enriched in P_1 cells (Defachelles et al., 2020). To determine whether NPP-21::GFP is also
202 enriched in P_1 cells, we quantified NPP-21::GFP fluorescence immediately following NEBD
203 (images labeled 20 seconds in Figure 2B). We performed this quantification at this stage of the
204 cell cycle since NPP-21::GFP localization was similar in both AB and P_1 cells immediately after
205 NEBD and entry into mitosis, in contrast to the changes in localization we observed at
206 metaphase in AB and P_1 cells (Figure 2B). When we performed this analysis, we detected more
207 NPP-21::GFP in P_1 cells than AB cells (Figure 2C). We were concerned that, even at this early
208 timepoint, the area occupied by NPP-21::GFP was different in AB and P_1 cells, potentially
209 affecting this quantification. To test this, we determined the area occupied by NPP-21::GFP
210 signal in AB and P_1 cells and found that this area was significantly smaller in P_1 cells than AB
211 cells (Figure 2D). Since AB and P1 cells show similar nuclear areas prior to NEBD (Gerhold et
212 al., 2018), this indicates that NPP-21::GFP is regulated differently in P_1 cells even at this early
213 timepoint. However, when we calculated the integrated intensity of NPP-21::GFP signal (Figure
214 2E) in both cell types, NPP-21::GFP signal was still significantly higher in P_1 cells than AB cells,
215 indicating that NPP-21::GFP is enriched in P_1 cells, potentially to drive the stronger checkpoint.
216
217 **NPP-21 concentrates PCH-2::GFP around mitotic chromosomes**
218
219 PCH-2 and its mammalian ortholog, Trip13, remodels active Mad2 to generate inactive Mad2
220 (Ye et al., 2015). This remodeling guarantees the availability of inactive Mad2 during checkpoint
221 activation so that the conversion of inactive Mad2 to active Mad2, and the production of soluble

222 MCC, is the rate limiting event in spindle checkpoint activation (Ma and Poon, 2016; Ma and
223 Poon, 2018; Nelson et al., 2015).
224
225 To evaluate whether NPP-21 contributed to the stronger spindle checkpoint in P_1 cells by
226 regulating PCH-2, we generated a strain that expresses both AID::NPP-21 and a fluorescently
227 tagged, functional PCH-2::GFP-3xFLAG (Nelson et al., 2015). Both *npp-21* and *pch-2* loci are
228 closely linked (0.20 cM apart). To generate the *AID::npp-21 pch-2::GFP-3xFLAG* double mutant
229 strain, the TIR1 transgene, also on the same chromosome, was crossed off in the recombination
230 event. Since we observed the defect in checkpoint strength in P_1 cells even in embryos that
231 have not been treated with auxin (Figure 1D), we first determined whether we could perform this
232 experiment in worms that did not express the TIR1 transgene. These double mutants do not
233 exhibit any embryonic inviability, indicating that the embryonic inviability we observe in *AID-*
234 *3xFLAG::npp-21 Pgld-1::TIR1-mRuby* strains on ethanol is likely the product of auxin-
235 independent but TIR1-dependent degradation of NPP-21 (Table 1). *AID-3xFLAG::npp-21 pch-*
236 *2::GFP-3xFLAG* hermaphrodites produced males at a higher, statistically significant frequency
237 than *pch-2::GFP-3xFLAG* animals*,* suggesting a very weak defect in meiotic chromosome
238 segregation (Table 1). However, *AID-3xFLAG::npp-21 pch-2::GFP-3xFLAG* embryos display a
239 stronger checkpoint in P_1 cells, similar to control animals (Figure 3A), indicating that *AID-*
240 *3xFlag::npp-21* is fully functional and the weaker checkpoint we observed in *3xFLAG::npp-21*
241 *Pgld-1::TIR1-mRuby* P1 cells was a product of TIR1 expression.
242
243 We introduced a different TIR1 transgene controlled by another germline promoter, *Psun-*
244 *1::TIR1-mRuby,* into strains with both *AID-3xFLAG::npp-21* and *pch-2::GFP-3xFLAG*
245 transgenes. Strains carrying AID::NPP-21, this transgenic version of TIR1 and PCH-2::GFP
246 showed a weaker spindle checkpoint in P_1 cells, similar to AB cells and in contrast to control
247 animals and strains with only AID::NPP-21 and PCH-2::GFP (Figure 3A). This phenotype was

248 also similar to the original strain expressing AID::NPP-21 and TIR1 via the *gld-1* promoter
249 (Figure 1D). When these worms were grown on plates containing ethanol, we observed an
250 increase in male self-progeny and no effect on viability (Table 1).
251
252 We quantified PCH-2::GFP in both AB and P_1 cells in embryos expressing AID::NPP-21 and
253 PCH-2::GFP with or without TIR1 (Figures 3B and C). Both strains showed statistically
254 significant enrichment of PCH-2::GFP in P_1 cells, compared to AB cells (Figure 3D). However,
255 we noticed that the area occupied by PCH-2::GFP increased in both AB and P_1 cells in strains
256 expressing TIR1, compared to strains without TIR1 (Figure 3E and Supplemental Figure 2).
257 Moreover, in P_1 cells without TIR1, the area occupied by PCH-2::GFP was larger than that
258 observed in AB cells without TIR1, likely because PCH-2::GFP often adopted a matrix-like
259 structure in P_1 cells (55%, 6 of 11 embryos) (Figure 3C and Supplemental Figure 2). However,
260 this structure was much less defined than the one observed with NPP-21::GFP (Figure 2B).
261 When the area occupied by PCH-2::GFP was used to calculate the integrated intensity of PCH-
262 2::GFP in AID::NPP-21 embryos with and without TIR1, P_1 cells in strains with TIR1 still had
263 higher levels of PCH-2::GFP but the comparison with AB cells was not statistically significant
264 (Figure 3F). This was in direct contrast to the experiments performed in embryos without TIR1
265 (Figure 3F). These data indicate that NPP-21 is not required to enrich PCH-2::GFP in P_1 cells
266 but instead, promotes its concentration around mitotic chromosomes in both AB and P_1 cells.
267 Given the defect in checkpoint strength in P_1 cells in this strain, we would argue that this
268 concentration is particularly important for the stronger checkpoint in P_1 cells. The inability to
269 properly concentrate PCH-2::GFP in P_1 cells may also explain why PCH-2::GFP rarely adopts a
270 matrix-like structure in P_1 cells in embryos expressing AID::NPP-21 and TIR1 (18%, 2 of 11
271 embryos) (Figure 3C and Supplemental Figure 2).
272
273 **NPP-21 promotes GFP::MAD-2 recruitment to unattached kinetochores in P_1 cells**

274

275 In both cultured *Drosophila* and human (HeLa) cells, NPP-21 orthologs, Megator and TPR
276 respectively, promote the localization of Mad2, but not Mad1, to unattached kinetochores by
277 acting as spatial regulators or ensuring protein stability (Lince-Faria et al., 2009; Schweizer et
278 al., 2013). To determine if NPP-21 plays a similar role in *C. elegans* embryos (Figures 4A and
279 B), we quantified GFP::MAD-2 at unattached kinetochores in *AID::npp-21* embryos (Figures 4B
280 and C). In AB cells, GFP::MAD-2 recruitment to unattached kinetochores was unaffected by
281 NPP-21 depletion (Figures 4B and C), consistent with their normal checkpoint activation (Figure
282 1C). P_1 cells treated with ethanol also showed normal GFP::MAD-2 recruitment, indicating that
283 the weaker spindle checkpoint in P_1 cells is not the result of a baseline defect in localizing Mad2
284 (Figures 4B and C). By contrast, NPP-21 depletion sharply reduced GFP::MAD-2 localization to
285 unattached kinetochores in P_1 cells (Figures 4B and C), demonstrating that the weaker
286 checkpoint response in these cells stems from the inability to robustly localize Mad2 to
287 unattached kinetochores.

288

289 During early development, embryos balance the rapid cell divisions of early embryogenesis with
290 the imperative of maintaining genomic integrity (Fusari and Milan, 2026), particularly in immortal
291 germline cells that will give rise to sperm and eggs. NPP-21, through its spindle matrix function,
292 contributes to this balance by promoting a stronger spindle checkpoint response in germline
293 cells, in contrast to somatic cells. The NPP-21 protein displays germline specific behavior: it is
294 enriched and consistently forms a spindle matrix in P_1 cells, suggesting a conserved
295 developmental role during embryogenesis. This function acts at two control points:
296 concentrating PCH-2 around mitotic chromosomes and promoting Mad2 recruitment to
297 unattached kinetochores. Because PCH-2 promotes the formation of inactive, open Mad2 for
298 checkpoint signaling, these two control points may be mechanistically linked. Whether other,

conserved spindle matrix components play similar, developmental, roles during embryogenesis is an interesting, open question for our future studies.

Materials and Methods

C. elegans Strains and Husbandry

The wildtype *C. elegans* strain background was Bristol N2 (Brenner, 1974) . All strains were maintained at 20°C. See Supplemental Table 1 for a list of all *C. elegans* strains used in this study.

The *AID::3xFLAG::npp-21* transgenic strain was generated by CRISPR/Cas9 genomic editing (Paix et al., 2017). Young adult worms carrying the *Pgld-1::Tir1mRuby::3'UTR(gld-1) (ieSi64)* transgene were injected with preassembled Cas9-RNP, 23 ng/µL of ssDNA repair template and 5 ng/uL pCFJ90 and 2.5 ng/uL pCFJ104 as co-injection markers. The target crRNA was TAGTCTTTCAGTTATGGATG (IDT) and the ssDNA repair template was generated by primer extension PCR using the following primer GTGTTATCTAATTAAATCTCTCAGTTCCTTCAAGTTATCATAT and gBlock CTCTCAGTTCCTTCAAGTTATCATATTTTTTAAGTAAAACTAATCGCCCGAAATTTAGTCTTTCA GTTATGCCTAAAGATCCAGCCAAACCTCCGGCCAAGGCACAAGTTGTGGGATGGCCACCG GTGAGATCATACCGGAAGAACGTGATGGTTTCCTGCCAAAAATCAAGCGGTGGCCCGGAG GCGGCGGCGTTCGTGAAGGACTATAAAGATCACGACGGAGATTACAAGGACCATGATATCG ACTACAAGGACGACGACGACAAGGGAGATGTGGATGCGCCACTTCAGGCGCCTGAACAAC CGGTCGCAGACGCTGACGATGAAGAAGCTAACTGGGAAATGGAAAAAGCCGAAATGAAAC GGATTGAG (both ordered from IDT). Transformants were identified and worms carrying the transgene were genotyped using the following primers: AATTGGCATCGCTGATCAATGAG and

324 GCTCTTTAATTTCAGCCGCATGAC. The presence of the insertion was verified by sequencing
325 and the transgenic strain was backcrossed at least three time before analysis.
326
327 **Viability and fertility**
328 To score total progeny and male self-progeny, L4 hermaphrodites were picked onto individual
329 plates with 1mM auxin, ethanol or no additional treatment, and transferred to new plates daily
330 over 4 days. The eggs laid on each plate were counted after removing the parent. Viable
331 progeny and male progeny were quantified when the F1 reached L4 or adult stages (2-3 days
332 post egg laying).
333
334 **Microscopy & Mitotic Timing Experiments**
335 All immunofluorescence and live microscopy was performed on a DeltaVision Personal DV
336 deconvolution microscope (Applied Precision) equipped with a 100X N.A. 1.40 oil-immersion
337 objective (Olympus) coupled with a CoolSNAP charge-coupled camera (Roper Scientific). For
338 live microscopy of two cell embryos, eggs were dissected 18-26 hours post-L4 into 1X Egg
339 Buffer (25mM Hepes pH7.4, 118uM NaCl, 48mM KCl, 2mM EDTA, 0.5mM EGTA) and mounted
340 on 2% agarose pads for immediate analysis. Environmental temperature was approximately
341 21°C during image collection. For mitotic timing experiments, Z-sections were acquired with 8x
342 2µm steps using a 100X objective (Olympus) at 20s intervals. Exposure time was 100ms for
343 mCherry::H2B and 50ms for GFP::PH. Mitotic duration was calculated for the AB cell in the
344 presence of monopolar spindles as the interval between NEBD to the onset of cortical
345 contractility (OCC) or the interval between NEBD and chromosome decondensation (DECON).
346 NEBD was defined by the equilibration of mCherry::H2B from the nucleus into the cytosol. OCC
347 was defined as the change in conformation of the plasma membrane from circular to rectangular
348 in AB cells, as anaphase in P_1 cells or as the first frame when a persistent membrane bleb
349 formed from the cortex of the embryo in *zyg-1*^{RNAi} embryos (Supplemental Figure 1A). DECON

350 was defined as the loss of punctate mCherry::H2B signal within the decondensing chromatin
351 (Supplemental Figure 1B). To minimize bleaching and maximize signal intensity of GFP-tagged
352 spindle checkpoint components (NPP-21, PCH-2 and MAD-2), imaging was started just after
353 NEBD as visualized by mCherry::H2B. Here, 8x 1µm steps were captured with 250ms GFP and
354 100ms mCherry exposures at 20s intervals.
355
356 Immunostaining was performed on worms 20–24 h after L4 stage, as described in (Russo et al.,
357 2021). Gonad dissections were performed in 1× EBT (250 mM Hepes-Cl, pH 7.4, 1.18 M NaCl,
358 480 mM KCl, 20 mM EDTA, and 5 mM EGTA) + 0.1% Tween 20 and 20 mM sodium azide. An
359 equal volume of 7.4% formaldehyde in EBT (final concentration was 3.7% formaldehyde) was
360 added and allowed to incubate under a coverslip for 5 min. The sample was mounted on
361 HistoBond slides (75 × 25 × 1 mm from VWR), freeze-cracked, and incubated in methanol at
362 −20°C for slightly more than 1 min and transferred to PBST (PBS with Tween 20). After several
363 washes of PBST, the samples were incubated for 30 min in 1% bovine serum albumin diluted in
364 PBST. A hand-cut paraffin square was used to cover the tissue with 50 µl of antibody solution.
365 Incubation was conducted in a humid chamber overnight at 4°C. Slides were rinsed in PBST
366 and then incubated for 2 h at room temperature with fluorophore-conjugated secondary antibody
367 at a dilution of 1:500. Samples were rinsed several times and DAPI stained in PBST, then
368 mounted in 13 µl of mounting media (20 M *N*-propyl gallate [Sigma-Aldrich] and 0.14 M Tris in
369 glycerol) with a no. 1 1/2 (22 mm^2) coverslip, and sealed with nail polish.
370
371 Mouse anti-FLAG [Sigma] primary antibodies were used for immunofluorescence at 1:1000 and
372 Alexa-Fluor 488 anti-mouse (Invitrogen) secondary antibodies were used at 1:500. Three-
373 dimensional image stacks were collected at 0.2-µm Z-spacing and processed by constrained,
374 iterative deconvolution. Image scaling and analysis were performed using functions in the
375 softWoRx software package. Projections were calculated by a maximum intensity algorithm.

376 Composite images were assembled and some false coloring was performed with Adobe
377 Photoshop.
378
379 **Quantification of NPP-21::GFP, GFP::MAD-2, and PCH-2::GFP-3XFLAG**
380 Analysis was performed in Fiji. Quantification of fluorescence around mitotic chromosomes was
381 quantified as described in (Defachelles et al., 2020). Sum intensity projections were generated
382 and average fluorescence in the area around mitotic chromosomes was measured in Fiji.
383 Background average fluorescence was measured in a 30-pixel band around this “cloud” and
384 subtracted from the initial fluorescence intensity to determine the final value. In some of our
385 movies to quantify PCH-2::GFP and localize NPP-21::GFP, identifying a clear metaphase plate
386 was more difficult in AB than in P1 cells. Therefore, to ensure that we were performing these
387 experiments at the same stage in mitosis in these two cell types, frames for the relevant
388 analysis were normalized relative to NEBD and mitotic exit.
389
390 Quantification of unattached kinetochore signal was performed essentially as described for
391 GFP::MAD-2 quantification in (Nelson et al., 2015). Maximum intensity projections of both
392 mCherry::H2B and GFP fusion proteins were made after the pseudo-metaphase plate was
393 generated. The image was rotated so the metaphase plate was vertical, channels were split,
394 and the maximum GFP pixel was identified using the process function within a box on the
395 unattached side of the metaphase plate. In the same x-plane, the maximum mCherry::H2B pixel
396 was found. The width was changed to 12 pixels and the maximum GFP signal intensity was
397 recorded in this 12 pixel window centered at the mCherry maxima. The background GFP signal
398 was calculated by taking the average GFP intensity of a 4 pixel box in the same x-plane, 8
399 pixels away from the maximum mCherry on the opposite side of the pseudo-metaphase plate to
400 the maximum GFP (i.e. the attached side). This background GFP was then subtracted from the

401 maximum to measure the kinetochore bound GFP fusion intensity. This process was repeated at
402 least 7x for each genetic background and treatment.
403
404 **Feeding RNA interference (RNAi)**
405 RNA interference (RNAi) was performed by growing relevant worm strains on HT115 bacteria
406 transformed with a vector allowing for IPTG inducible expression of dsRNA against the *zyg-1*
407 gene. Bacterial strains containing this RNAi vector were cultured overnight at 37°C, centrifuged,
408 and the pellet was re-suspended in 1/10 of the original volume. 50uL of concentrated culture
409 was spotted onto a nematode growth medium (NGM) plate with 1mM IPTG and 50ug/uL of
410 kanamycin and the RNAi spot was allowed to grow overnight at 37°C. Plates were stored at 4°C
411 for up to 10 days.
412
413 L4 hermaphrodite worms were transferred to RNAi plates, allowed to incubate for 2–3 hours,
414 and then transferred to fresh RNAi plates. Live microscopy was performed on embryos 22–26
415 hours after worms were picked to the *zyg-1* RNAi plate. HT115 bacteria transformed with
416 pHSG298 (Clontech) was used as a control for $zyg\text{-}1^{RNAi}$.
417
418 **Auxin treatment**
419 Auxin treatment was performed on worms 20–24 hours after L4 stage by transferring worms to
420 bacteria-seeded plates containing auxin or ethanol. The natural auxin indole-3-acetic acid (IAA)
421 was purchased from Alfa Aesar (#A10556). A 100 mM stock solution in ethanol was prepared
422 and was stored at 4°C for up to two months. 100ul of the auxin stock solution or ethanol was
423 added to NGM plates (volume 10mls) to achieve a final concentration of 1mM.
424
425 To perform RNAi against *zyg-1* and auxin treatment, L4 hermaphrodite worms were transferred
426 to RNAi plates, allowed to incubate for 2–3 hours, and then transferred to fresh RNAi plates for

427 20-22 hours. Worms were then transferred to RNAi plates containing either auxin or ethanol to
428 incubate for 2-3 hours before performing live microscopy.
429
430 **Statistical Analysis**
431 Data was analyzed using Prism for statistical significance. For Figures 2C, D and E, student's t-
432 test was used to assess significance. For all other data, one-way ANOVA with Šídák correction
433 was used to assess significance.
434
435 **Acknowledgements**
436 We would like to thank Arshad Desai, Karen Oegema, Peter Askjaer and Geraldine Seydoux for
437 valuable *C. elegans* strains. We thank the members of the Bhalla lab for reading of the
438 manuscript. This work and the resulting manuscript was supported by the National Institutes of
439 Health (NIH) (grant numbers R35GM141835 [N.B.], T32GM133391 [S.B.] and R01GM065591
440 [A.F.D.]), a postdoctoral fellowship of the Human Frontier Science Program (LT000903/2013-C
441 [S.K.]) and the Howard Hughes Medical Institute (A.F.D.). Some strains were provided by the
442 CGC, which is funded by NIH Office of Research Infrastructure Programs (P40 OD010440).
443
444 Because this manuscript is the result of funding in whole or in part by the NIH, this manuscript is
445 subject to the NIH Public Access Policy. Through acceptance of this federal funding, NIH has
446 been given a right to make this manuscript publicly available in PubMed Central upon the
447 Official Date of Publication.
448
449

450 **References**

451

452 Baker, D.J., K.B. Jeganathan, J.D. Cameron, M. Thompson, S. Juneja, A. Kopecka, R. Kumar,
453 R.B. Jenkins, P.C. de Groen, P. Roche, and J.M. van Deursen. 2004. BubR1
454 insufficiency causes early onset of aging-associated phenotypes and infertility in mice.
455 *Nat Genet*. 36:744-749.

456 Brenner, S. 1974. The genetics of Caenorhabditis elegans. *Genetics*. 77:71-94.

457 Cohen-Fix, O., and P. Askjaer. 2017. Cell Biology of the Caenorhabditis elegans Nucleus.
458 *Genetics*. 205:25-59.

459 Collin, P., O. Nashchekina, R. Walker, and J. Pines. 2013. The spindle assembly checkpoint
460 works like a rheostat rather than a toggle switch. *Nat Cell Biol*. 15:1378-1385.

461 Defachelles, L., A.E. Russo, C.R. Nelson, and N. Bhalla. 2020. The conserved AAA-ATPase
462 PCH-2 (TRIP13) regulates spindle checkpoint strength. *Mol Biol Cell*. 31:2219-2233.

463 Essex, A., A. Dammermann, L. Lewellyn, K. Oegema, and A. Desai. 2009. Systematic analysis
464 in Caenorhabditis elegans reveals that the spindle checkpoint is composed of two largely
465 independent branches. *Mol Biol Cell*. 20:1252-1267.

466 Fusari, E., and M. Milan. 2026. Developmental tolerance and disease implications of
467 aneuploidy. *Curr Biol*. 36:R210-R228.

468 Galli, M., and D.O. Morgan. 2016. Cell Size Determines the Strength of the Spindle Assembly
469 Checkpoint during Embryonic Development. *Dev Cell*. 36:344-352.

470 Gerhold, A.R., V. Poupart, J.C. Labbe, and P.S. Maddox. 2018. Spindle assembly checkpoint
471 strength is linked to cell fate in the Caenorhabditis elegans embryo. *Mol Biol Cell*.
472 29:1435-1448.

473 Huang, L., W. Li, X. Dai, S. Zhao, B. Xu, F. Wang, R.T. Jin, L. Luo, L. Wu, X. Jiang, Y. Cheng, J.
474 Zou, C. Xu, X. Tong, H.Y. Fan, H. Zhao, and J. Bao. 2023. Biallelic variants in

475 MAD2L1BP (p31(comet)) cause female infertility characterized by oocyte maturation
476 arrest. *Elife*. 12.
477 Kops, G.J., B.A. Weaver, and D.W. Cleveland. 2005. On the road to cancer: aneuploidy and the
478 mitotic checkpoint. *Nat Rev Cancer*. 5:773-785.
479 Kyogoku, H., and T.S. Kitajima. 2017. Large Cytoplasm Is Linked to the Error-Prone Nature of
480 Oocytes. *Dev Cell*. 41:287-298 e284.
481 Lara-Gonzalez, P., J. Pines, and A. Desai. 2021. Spindle assembly checkpoint activation and
482 silencing at kinetochores. *Semin Cell Dev Biol*. 117:86-98.
483 Lince-Faria, M., S. Maffini, B. Orr, Y. Ding, F. Claudia, C.E. Sunkel, A. Tavares, J. Johansen,
484 K.M. Johansen, and H. Maiato. 2009. Spatiotemporal control of mitosis by the conserved
485 spindle matrix protein Megator. *J Cell Biol*. 184:647-657.
486 Ma, H.T., and R.Y. Poon. 2016. TRIP13 Regulates Both the Activation and Inactivation of the
487 Spindle-Assembly Checkpoint. *Cell Rep*. 14:1086-1099.
488 Ma, H.T., and R.Y.C. Poon. 2018. TRIP13 Functions in the Establishment of the Spindle
489 Assembly Checkpoint by Replenishing O-MAD2. *Cell Rep*. 22:1439-1450.
490 Matthews, H.K., C. Bertoli, and R.A.M. de Bruin. 2022. Cell cycle control in cancer. *Nat Rev Mol*
491 *Cell Biol*. 23:74-88.
492 Nelson, C.R., T. Hwang, P.H. Chen, and N. Bhalla. 2015. TRIP13PCH-2 promotes Mad2
493 localization to unattached kinetochores in the spindle checkpoint response. *J Cell Biol*.
494 211:503-516.
495 Nishimura, K., T. Fukagawa, H. Takisawa, T. Kakimoto, and M. Kanemaki. 2009. An auxin-based
496 degron system for the rapid depletion of proteins in nonplant cells. *Nat Methods*. 6:917-
497 922.
498 O'Connell, K.F., C. Caron, K.R. Kopish, D.D. Hurd, K.J. Kemphues, Y. Li, and J.G. White. 2001.
499 The C. elegans zyg-1 gene encodes a regulator of centrosome duplication with distinct
500 maternal and paternal roles in the embryo. *Cell*. 105:547-558.

501 Paix, A., A. Folkmann, and G. Seydoux. 2017. Precision genome editing using CRISPR-Cas9
502 and linear repair templates in C. elegans. *Methods*. 121-122:86-93.
503 Piano, F., A.J. Schetter, M. Mangone, L. Stein, and K.J. Kemphues. 2000. RNAi analysis of
504 genes expressed in the ovary of Caenorhabditis elegans. *Curr Biol*. 10:1619-1622.
505 Qi, H., U. Rath, D. Wang, Y.Z. Xu, Y. Ding, W. Zhang, M.J. Blacketer, M.R. Paddy, J. Girton, J.
506 Johansen, and K.M. Johansen. 2004. Megator, an essential coiled-coil protein that
507 localizes to the putative spindle matrix during mitosis in Drosophila. *Mol Biol Cell*.
508 15:4854-4865.
509 Robertson, S., and R. Lin. 2013. The oocyte-to-embryo transition. *Adv Exp Med Biol*. 757:351-
510 372.
511 Russo, A.E., C.R. Nelson, and N. Bhalla. 2021. Mutating two putative phosphorylation sites on
512 ZHP-3 does not affect its localization or function during meiotic chromosome
513 segregation. *MicroPubl Biol*. 2021.
514 Schweizer, N., C. Ferras, D.M. Kern, E. Logarinho, I.M. Cheeseman, and H. Maiato. 2013.
515 Spindle assembly checkpoint robustness requires Tpr-mediated regulation of
516 Mad1/Mad2 proteostasis. *J Cell Biol*. 203:883-893.
517 Thomas, L., B. Taleb Ismail, P. Askjaer, and G. Seydoux. 2023. Nucleoporin foci are stress-
518 sensitive condensates dispensable for C. elegans nuclear pore assembly. *EMBO J*.
519 42:e112987.
520 Ye, Q., S.C. Rosenberg, A. Moeller, J.A. Speir, T.Y. Su, and K.D. Corbett. 2015. TRIP13 is a
521 protein-remodeling AAA+ ATPase that catalyzes MAD2 conformation switching. *eLife*. 4.
522 Zhang, L., J.D. Ward, Z. Cheng, and A.F. Dernburg. 2015. The auxin-inducible degradation
523 (AID) system enables versatile conditional protein depletion in C. elegans. *Development*.
524 142:4374-4384.
525 Zhang, Z., B. Li, J. Fu, R. Li, F. Diao, C. Li, B. Chen, J. Du, Z. Zhou, J. Mu, Z. Yan, L. Wu, S. Liu,
526 W. Wang, L. Zhao, J. Dong, L. He, X. Liang, Y. Kuang, X. Sun, Q. Sang, and L. Wang.

527 2020. Bi-allelic Missense Pathogenic Variants in TRIP13 Cause Female Infertility
528 Characterized by Oocyte Maturation Arrest. *Am J Hum Genet*. 107:15-23.
529 Zheng, Y. 2010. A membranous spindle matrix orchestrates cell division. *Nat Rev Mol Cell Biol*.
530 11:529-535.
531

532 **Table 1: Viability of strains**

533

534 **Figure Legends**

535

536 **Figure 1: NPP-21 is required for the stronger spindle checkpoint in germline cells of the**
537 **two-cell embryo.** A. AID-3xFLAG::NPP-21 is degraded in oocytes after one hour of auxin
538 treatment. Images of cellularized (-1) oocytes from worms treated with ethanol or auxin stained
539 with antibodies against the FLAG tag and DAPI to visualize DNA. Scale bar indicates 5 microns.
540 B. Cartoon indicating a two cell embryo with the AB and P_1 cell labeled and the nucleus colored
541 magenta. C. AID-3XFLAG::NPP-21 is functional and not required for the spindle checkpoint in
542 AB, somatic, cells. Graph depicting mitotic timing in AB cells of embryos treated with ethanol or
543 auxin and control RNAi or *zyg-1* RNAi. D. AID-3XFLAG::NPP-21 cannot support the stronger
544 checkpoint and is required for a robust spindle checkpoint in P_1, germline, cells. Graph
545 depicting mitotic timing in P_1 cells of embryos treated with ethanol or auxin and control RNAi or
546 *zyg-1* RNAi. In all graphs, a * indicates a p value < 0.05, a ** indicates a p value < 0.01, a ***
547 indicates a p value < 0.001, a **** indicates a p value < 0.0001, ns indicates not significant and
548 error bars indicate 95% confidence intervals.

549

550 **Figure 2: NPP-21::GFP is enriched in P_1, germline, cells and its localization is distinct**
551 **from that in AB, somatic, cells.** A. NPP-21::GFP is functional for the spindle checkpoint in AB
552 and P_1 cells. A graph depicting mitotic timing in AB and P_1 cells of control and *npp-21::GFP*
553 animals treated with control and *zyg-1* RNAi. B. NPP-21::GFP localization in P_1 cells is different
554 than in AB cells in most two cell embryos. Images of AB and P_1 cells expressing mCherry::H2B
555 (magenta) and NPP-21::GFP (green) at NEBD, 20 seconds after NEBD and at metaphase (120
556 seconds after NEBD). C. NPP-21::GFP is asymmetrically enriched in P_1 cells. Graph depicting
557 average fluorescence of NPP-21::GFP in AB and P_1 cells 20 seconds after NEBD. D. The area

558 occupied by NPP-21::GFP is smaller in P_1 cells. Graph depicting the area in microns^2 of NPP-
559 21::GFP in AB and P_1 cells 20 seconds after NEBD. E. NPP-21::GFP is asymmetrically enriched
560 in P_1 cells. Graph depicting integrated intensity of NPP-21-::GFP in AB and P_1 cells 20 seconds
561 after NEBD.
562
563 **Figure 3: NPP-21 concentrates PCH-2::GFP around mitotic chromosomes in both AB and**
564 **P_1 cells.** A. Worms expressing both AID-3XFLAG::NPP-21 and TIR1 cannot support the
565 stronger checkpoint. A graph depicting mitotic timing in AB and P_1 cells of control, *AID::npp-21*
566 and *AID::npp-21;TIR1* animals treated with control and *zyg-1* RNAi. B. Cartoon of PCH-2::GFP
567 localization in AB and P_1 cells. C. Images of PCH-2::GFP (green) localization in AB and P_1 cells
568 expressing mCherry::H2B (magenta) in metaphase, in embryos without and with the TIR1 gene.
569 Scale bar indicates 5 microns. D. PCH-2::GFP is asymmetrically enriched in P_1 cells, in
570 embryos without and with the TIR1 gene. Graph depicting average fluorescence of PCH-2::GFP
571 in AB and P_1 cells at metaphase. E. The area occupied by PCH-2::GFP is greater in AB and P_1
572 cells in embryos expressing TIR1. Graph depicting the area in microns^2 of PCH-2::GFP in AB
573 and P_1 cells in metaphase. E. PCH-2::GFP is less concentrated in AB and P_1 cells of embryos
574 expressing TIR1. Graph depicting integrated intensity of PCH-2::GFP in AB and P_1 cells.
575
576 **Figure 4: NPP-21 is required for GFP::MAD-2 recruitment to unattached kinetochores in**
577 **P_1, germline, cells.** A. Cartoon of GFP::MAD-2 localization in AB and P_1 cells in *zyg-1^{RNAi}*
578 embryos. B. Images of GFP::MAD-2 (green) localization in AB and P_1 cells in *zyg-1^{RNAi}* embryos
579 expressing mCherry::H2B (magenta), treated with ethanol (top) or auxin (bottom). Scale bar
580 indicates 5 microns. C. Quantification of GFP::MAD-2 in AB and P_1 cells at unattached
581 kinetochores in *zyg-1^{RNAi}* embryos treated with ethanol or auxin.
582

583 **Supplemental Figure 1:** A. Images of AB and P_1 cells expressing mCherry::H2B (magenta) and
584 GFP::PH (green) at NEBD or OCC in control or *zyg-1*^{RNAi} embryos. B. Grayscale images of
585 mCherry::H2B in control or *zyg-1*^{RNAi} embryos. Scale bars indicate 5 microns.
586
587 **Supplemental Figure 2: Grayscale images of PCH-2::GFP in *AID::npp-21* strains without**
588 **(top) and with TIR1 (bottom).** Area of enrichment indicated by yellow dotted circle. Scale bar
589 indicates 5 microns.
590
591 **Supplemental Movie 1: In 75% of *C. elegans* two-cell embryos, NPP-21::GFP forms a**
592 **spindle matrix only in P_1 cells.** A two cell embryo expressing mCherry::H2B (red) and NPP-
593 21::GFP (green) undergoing mitosis. The AB cell divides first and is on the right and the P_1 cell
594 divides after the AB cell and is on the left.
595
596 **Supplemental Movie 2: In 25% of *C. elegans* two-cell embryos, NPP-21::GFP forms a**
597 **spindle matrix in both AB and P_1 cells.** A two cell embryo expressing mCherry::H2B (red) and
598 NPP-21::GFP (green) undergoing mitosis. The AB cell divides first and is on the right and the P_1
599 cell divides after the AB cell and is on the left.
600
601 **Supplemental Table 1: *C. elegans* strains used in this study**
602

Table 1: Viability of strains

Genotype and condition	Embryonic viability (number of embryos)	% Males
mCherry::H2B; GFP::PH + ethanol	100% (2165)	0.05%
mCherry::H2B; GFP::PH + auxin	100% (1799)	0.08%
AID-3xFLAG::npp-21 Pgld-1::TIR-1-mRuby; mCherry::H2B; GFP::PH + ethanol	96% (2245)****	2.3%****
AID-3xFLAG::npp-21 Pgld-1::TIR-1-mRuby; mCherry::H2B; GFP::PH + auxin	0.25% (1598)****	25%****
pch-2::GFP-3xFLAG; mCherry::H2B	100% (3061)	0.06%
AID-3xFLAG::npp-21 pch-2::GFP-3xFLAG; mCherry::H2B	100% (3373)	0.6%***
AID-3xFLAG::npp-21 pch-2::GFP-3xFLAG; Psun-1::TIR-1-mRuby mCherry::H2B + ethanol	100% (2113)	1.7%****

A *** indicates a P value < 0.001 and a **** indicates a P value < 0.0001

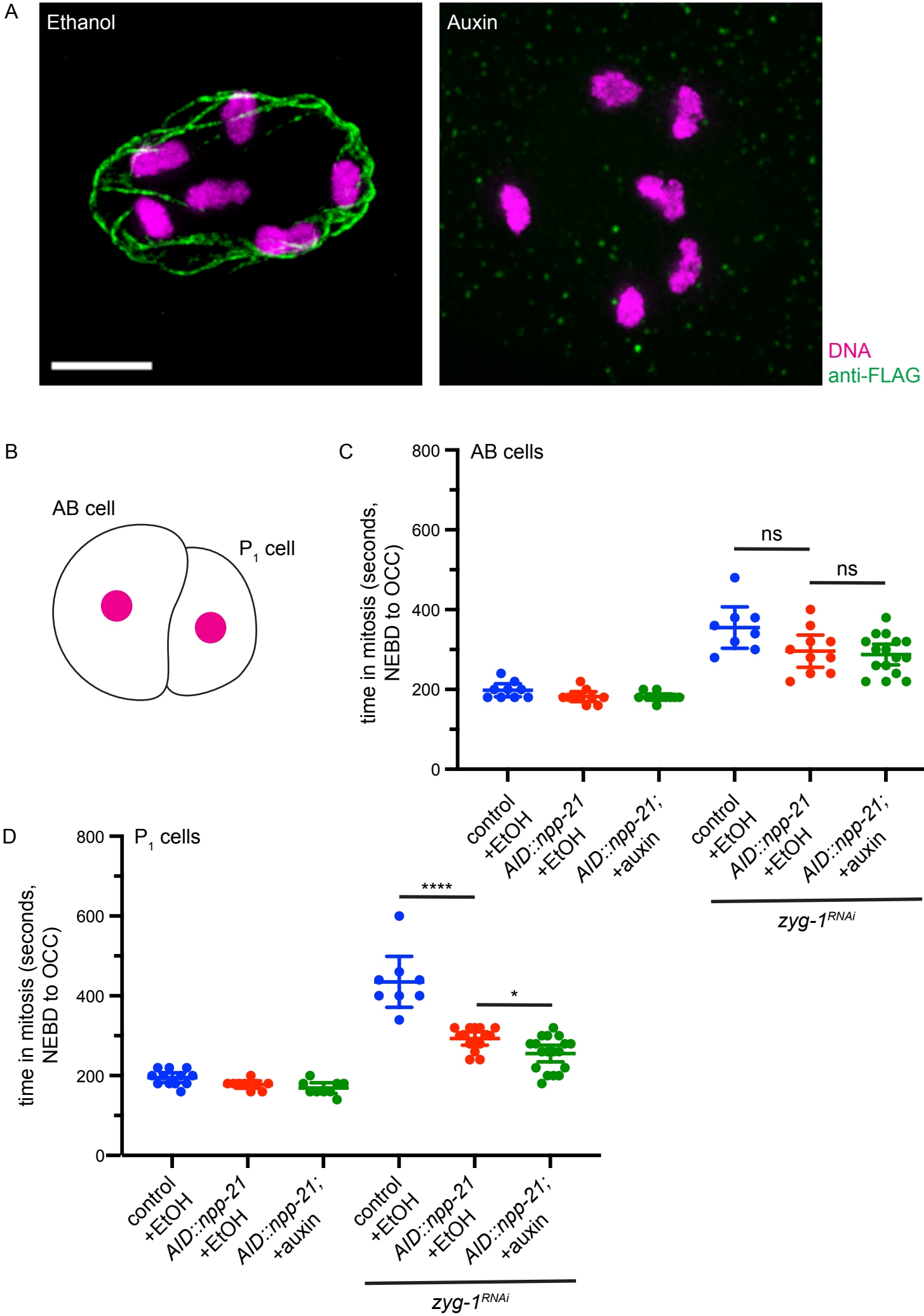
A
Ethanol
Auxin
DNA
anti-FLAG
B
AB cell
P1 cell
C
AB cells
time in mitosis (seconds, NEBD to OCC)
800
600
400
200
0
ns
ns
control +EtOH
AID::npp-21 +EtOH
AID::npp-21; +auxin
control +EtOH
AID::npp-21 +EtOH
AID::npp-21; +auxin
zyg-1RNAi
D
P1 cells
time in mitosis (seconds, NEBD to OCC)
800
600
400
200
0
****
*
control +EtOH
AID::npp-21 +EtOH
AID::npp-21; +auxin
control +EtOH
AID::npp-21 +EtOH
AID::npp-21; +auxin
zyg-1RNAi

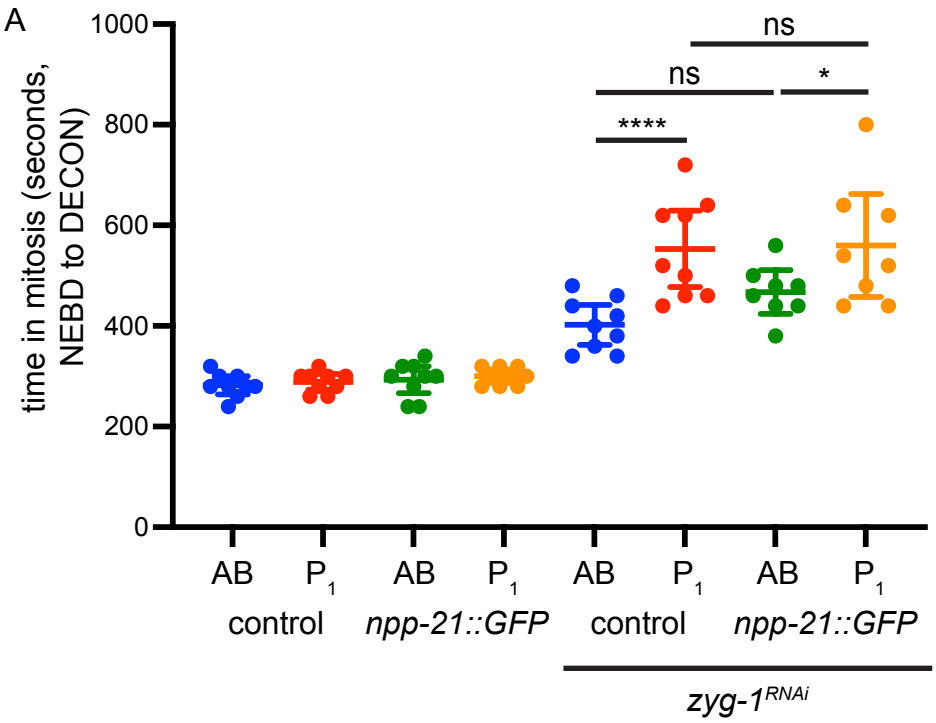
A
time in mitosis (seconds, NEBD to DECON)
1000
800
600
400
200
0
ns
ns
*
****
AB
P1
AB
P1
AB
P1
AB
P1
control
npp-21::GFP
control
npp-21::GFP
zyg-1RNAi

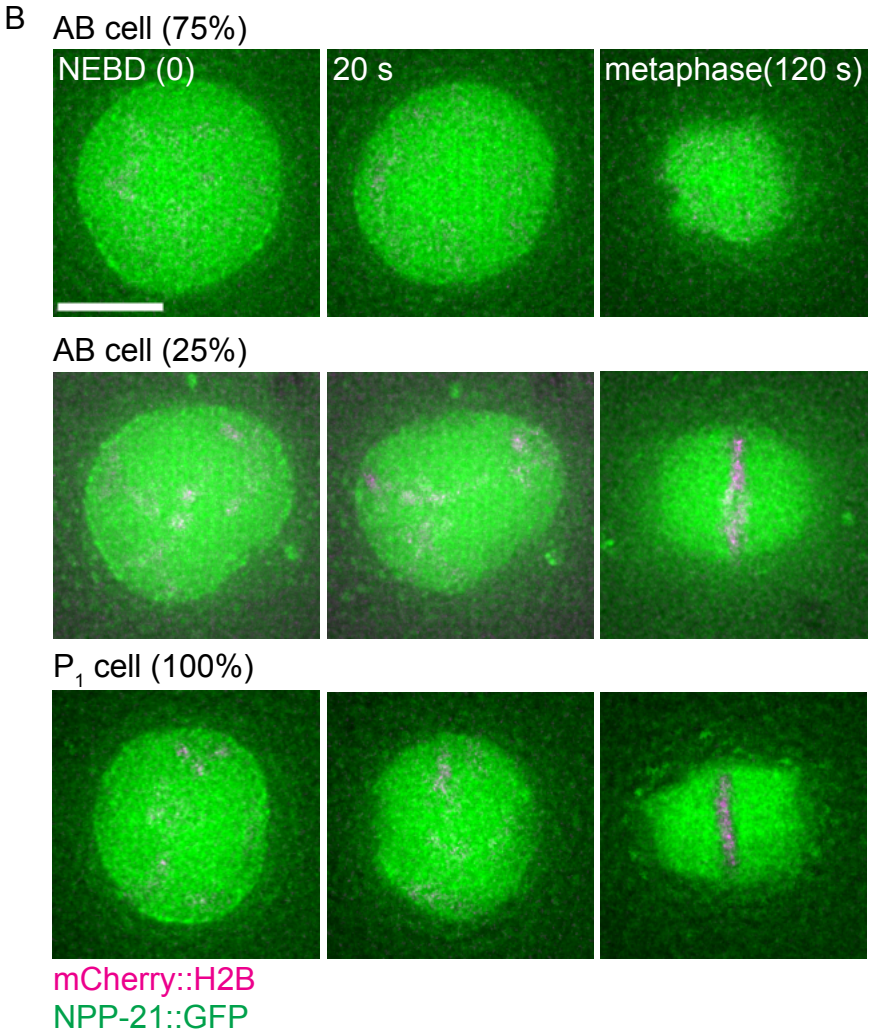
B
AB cell (75%)
NEBD (0)
20 s
metaphase(120 s)
AB cell (25%)
P1 cell (100%)
mCherry::H2B
NPP-21::GFP

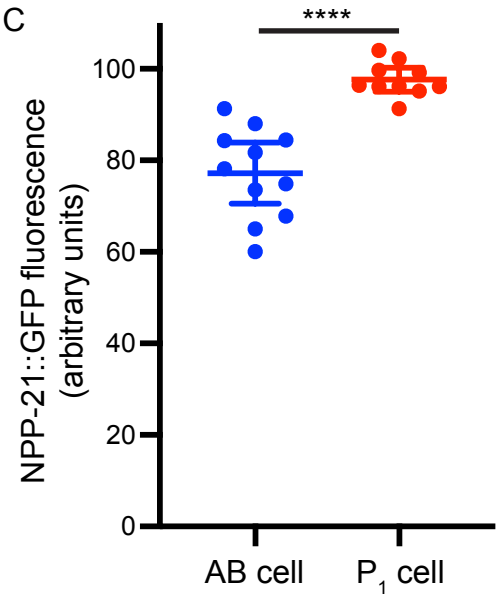
C
NPP-21::GFP fluorescence (arbitrary units)
100
80
60
40
20
0
****
AB cell
P1 cell

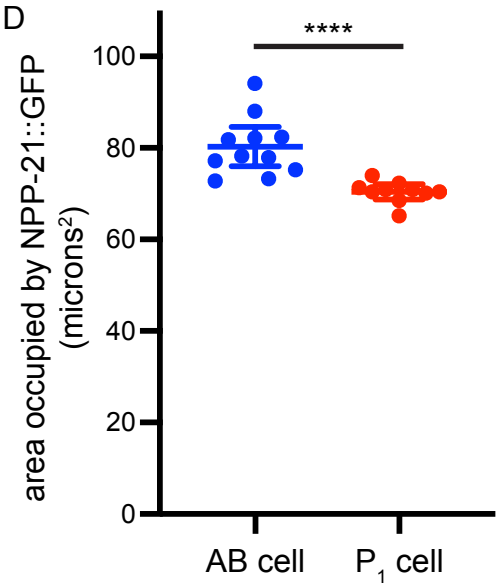
D
area occupied by NPP-21::GFP (microns2)
100
80
60
40
20
0
****
AB cell
P1 cell

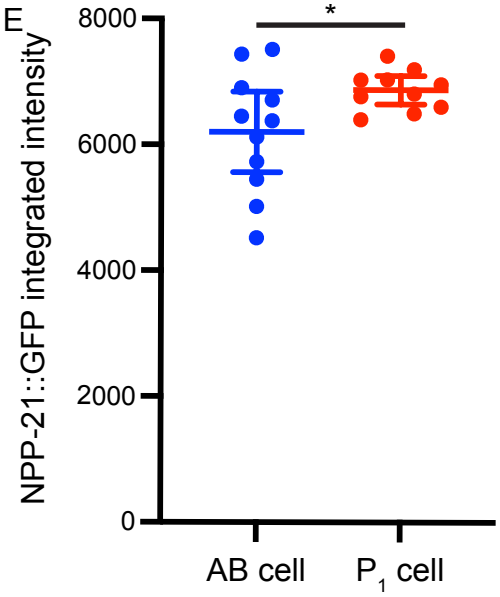
E
NPP-21::GFP integrated intensity
8000
6000
4000
2000
0
*
AB cell
P1 cell

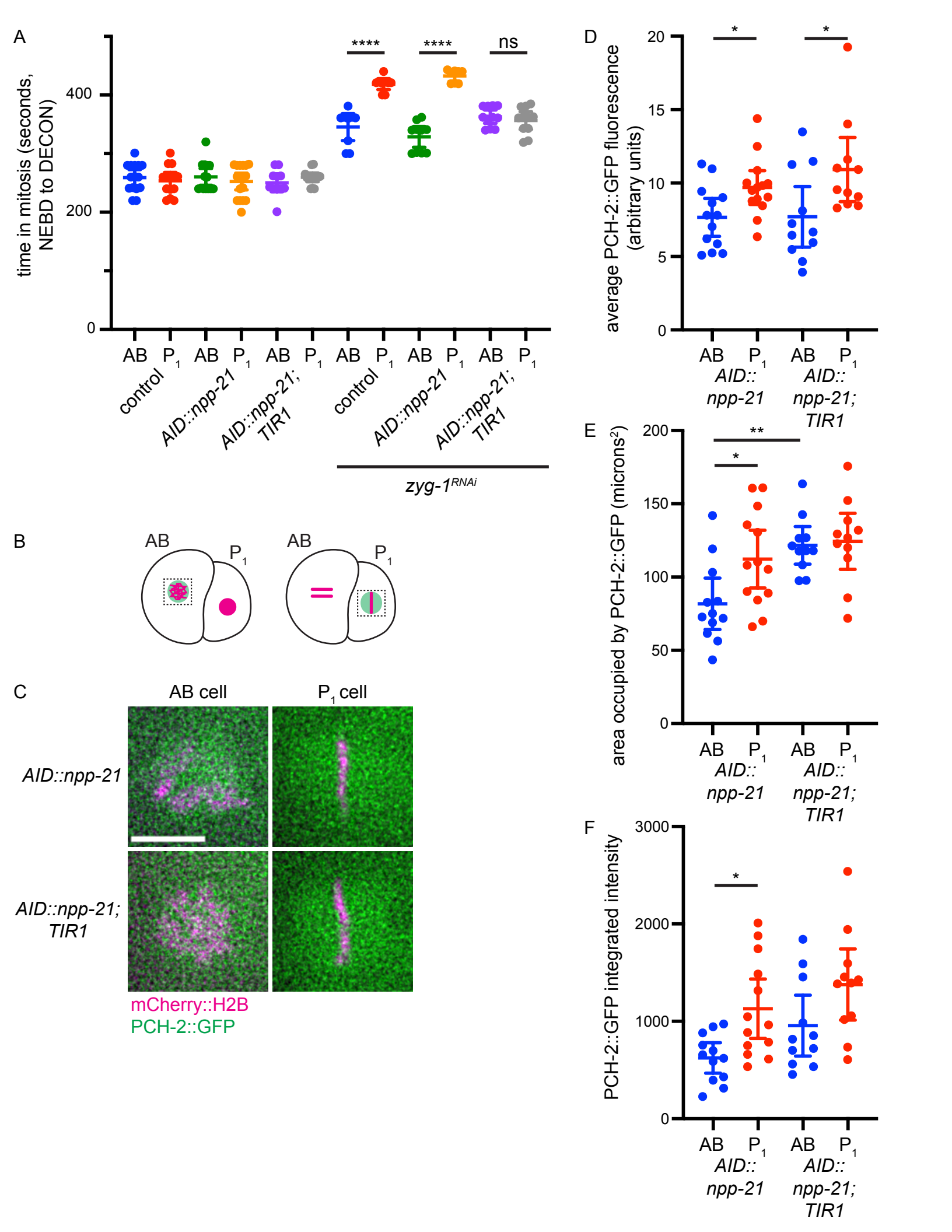
A
time in mitosis (seconds, NEBD to DECON)
0
200
400
****
****
ns
AB
P1
control
AID::npp-21
AID::npp-21; TIR1
zyg-1RNAi
B
AB
P1
C
AB cell
P1 cell
AID::npp-21
AID::npp-21; TIR1
mCherry::H2B
PCH-2::GFP
D
average PCH-2::GFP fluorescence (arbitrary units)
0
5
10
15
20
*
*
AID:: npp-21
AID:: npp-21; TIR1
E
area occupied by PCH-2::GFP (microns2)
0
50
100
150
200
**
*
F
PCH-2::GFP integrated intensity
0
1000
2000
3000
*

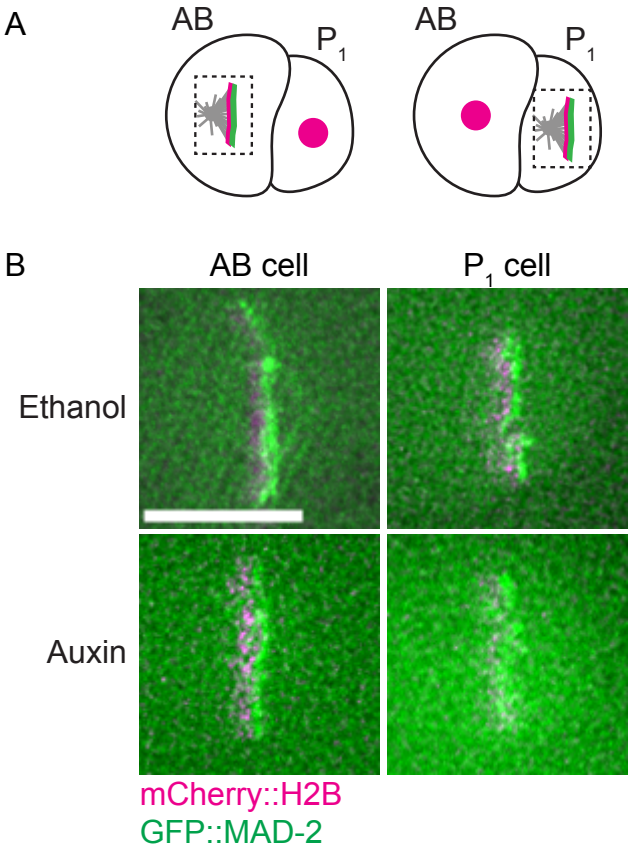
A
AB
P1
AB
P1
B
AB cell
P1 cell
Ethanol
Auxin
mCherry::H2B
GFP::MAD-2

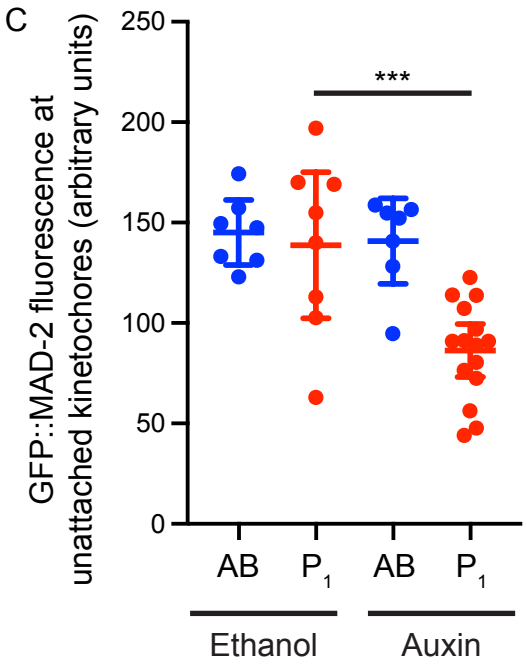
C
GFP::MAD-2 fluorescence at unattached kinetochores (arbitrary units)
250
200
150
100
50
0
***
AB
P1
AB
P1
Ethanol
Auxin